Received: 22 April 2023 | Revised: 16 August 2023 | Accepted: 13 October 2023

DOI: 10.1096/fj.202300799R

RESEARCH ARTICLE

The FASEB Journal

Alteration of cholesterol content and oxygen level in intestinal organoids after infection with *Staphylococcus aureus*

AhmedElmontaser Mergani[1,2] | **Marita Meurer**[1,2] | **Elena Wiebe**[3] | **Katrin Dümmer**[1,2] | **Katrin Wirz**[1,2] | **Judith Lehmann**[3] | **Graham Brogden**[1,2] | **Maren Schenke**[3] | **Katrin Künnemann**[4] | **Hassan Y. Naim**[1] | **Guntram A. Grassl**[4] | **Maren von Köckritz-Blickwede**[1,2] | **Bettina Seeger**[3]

[1]Institute of Biochemistry, University of Veterinary Medicine Hannover, Hannover, Germany

[2]Research Center for Emerging Infections and Zoonoses (RIZ), University of Veterinary Medicine Hannover, Hannover, Germany

[3]Institute for Food Quality and Food Safety, Research Group Food Toxicology and Replacement/Complementary Methods to Animal Testing, University of Veterinary Medicine Hannover, Hannover, Germany

[4]Institute of Medical Microbiology and Hospital Epidemiology and German Center for Infection Research (DZIF), Partner Site Hannover, Hannover Medical School, Hannover, Germany

Correspondence
Maren von Köckritz-Blickwede, Institute of Biochemistry, University of Veterinary Medicine Hannover, Hannover, Germany.
Email: maren.von.koeckritz-blickwede@tiho-hannover.de

Bettina Seeger, Institute for Food Quality and Food Safety, Research Group Food Toxicology and Replacement/Complementary Methods to Animal Testing, University of Veterinary Medicine Hannover, Hannover, Germany.
Email: bettina.seeger@tiho-hannover.de

Funding information
Niedersächsisches Ministerium für Wissenschaft und Kultur (MWK), Grant/Award Number: 74ZN1574; Niedersächsiches Ministerium für

Abstract

The pathogenicity elicited by *Staphylococcus* (*S.*) *aureus*, one of the best-studied bacteria, in the intestine is not well understood. Recently, we demonstrated that *S. aureus* infection induces alterations in membrane composition that are associated with concomitant impairment of intestinal function. Here, we used two organoid models, induced pluripotent stem cell (iPSC)-derived intestinal organoids and colonic intestinal stem cell-derived intestinal organoids (colonoids), to examine how sterol metabolism and oxygen levels change in response to *S. aureus* infection. HPLC quantification showed differences in lipid homeostasis between infected and uninfected cells, characterized by a remarkable decrease in total cellular cholesterol. As the altered sterol metabolism is often due to oxidative stress response, we next examined intracellular and extracellular oxygen levels. Three different approaches to oxygen measurement were applied: (1) cell-penetrating nanoparticles to quantify intracellular oxygen content, (2) sensor plates to quantify extracellular oxygen content in the medium, and (3) a sensor foil

Abbreviations: 25(R)27-HC, 25(R)-27-hydroxycholesterol; 25-HC, 25-hydroxy-cholesterol; 4β-HC, 4β-hydroxycholesterol; 7-OC, 7-keto-cholesterol; 7β-HC, 7β-hydroxycholesterol; BBM, brush border membrane; BHT, butylhydroxytoluol; CFU, colony-forming units; CHGA, chromogranin A; ECM, extracellular matrix; EDTA, ethylenediaminetetraacetic acid; HPLC, high-performance liquid chromatography; iPSC, induced pluripotent stem cell; LGR5, leucine-rich repeat-containing G-protein coupled receptor 5; LPS, lipopolysaccharide; LYZ, lysozyme; mDF, modified Davidson's fluid; MOI, multiplicity of infection; MUC2, mucin 2; PAS, periodic acid Schiff; PBS, phosphate-buffered saline; PFA, paraformaldehyde; PPIA, cyclophilin A; RPS23, ribosomal protein S23; SI, sucrase-isomaltase; SOX9, SRY-Box Transcription Factor 9.

Wissenschaft und Kultur, Grant/Award Number: ZukunftNiedersachsen, MikroReplaceSystems

system for oxygen distribution in organoid cultures. The data revealed significant intracellular and extracellular oxygen drop after infection in both intestinal organoid models as well as in Caco-2 cells, which even 48 h after elimination of extracellular bacteria, did not return to preinfection oxygen levels. In summary, we show alterations in sterol metabolism and intra- and extracellular hypoxia as a result of *S. aureus* infection. These results will help understand the cellular stress responses during sustained bacterial infections in the intestinal epithelium.

KEYWORDS

HPLC, intestinal organoids, oxygen measurement, oxysterols, *S. aureus* Newman, stem cells

1 | INTRODUCTION

Staphylococcus (S.) aureus is a multifaceted and an opportunistic pathogen that can live as a commensal organism on the skin, in the nose, and throat. It is known for its impact as a nosocomial and community acquired pathogen, therefore extensive investigations of this pathogen have been conducted over the recent years.[1] The infection can involve any organ and can cause a broad spectrum of symptoms, including boils, abscess formation, wound infections, endocarditis, osteomyelitis, and sepsis or septic shock and it can also be a frequent pathogen of foreign body infections.[2] It is also often responsible for toxin-mediated diseases, such as toxic shock syndrome, scaled skin syndrome, and staphylococcal foodborne disease (SFD).[3] Staphylococcus foodborne disease is caused by the ingestion of food contaminated with *S. aureus*, which produces heat-stable enterotoxins that bind to and stimulate the gastrointestinal epithelium, leading to symptoms such as nausea, vomiting, and diarrhea.[4] Furthermore, using a mouse model various *S. aureus* strains have been shown to colonize the intestinal tract and contribute to damage in the small intestine.[5] Although SFD is one of the most common food borne disease worldwide, very little is known about the role of the intact bacteria in the pathophysiology of the symptoms.

Given the increasing need and limited information available to understand the molecular pathophysiological mechanisms underlying *S. aureus* infection in the gastrointestinal tract, a predictable model is ultimately required. Caco-2 cells have been frequently utilized as an intestinal cellular model, since they express upon differentiation phenotypic characteristics of the epithelium from the intestinal tract. They acquire strict polarized morphology that is characterized by the existence of two structurally and functionally distinct apical and basolateral membranes. They also express tight junctions, transporters, and enzymes characteristic of absorptive enterocytes. Typical membrane proteins of the apical membrane include small intestinal hydrolases, such as sucrose-isomaltase (SI), aminopeptidase N, and dipeptidyl peptidase IV, and also transporters such as sodium-glucose transporter 1.[6]

In recent years, human stem cell-derived intestinal organoids have been proposed as a novel in vitro model that better mimic the in vivo situation in comparison to classical intestinal cell lines, such as Caco-2 or HT-29 cells. Intestinal organoids comprise in addition to absorptive enterocytes, goblet cells, enteroendocrine cells, Paneth cells, and intestinal stem cells.[7] 3D organoids represent an exquisite connection between 2D monolayer cultures and animal models. The higher the complexity of the experimental setup, according to Aguilar and colleagues,[7] the more complex and specific are the interactions between cell types and organ systems with pathogens.

The available model systems have both advantages and disadvantages, which were extensively reviewed by Rahman et al.[8] On one hand, classical human intestinal cell lines primarily represent absorptive enterocytes, which are the most abundant cell type in the intestinal epithelium. These cell lines form a polarized epithelium in 2D cell culture, allowing easy access to the apical side. On the other hand, intestinal organoids derived from stem cells contain a variety of specialized cells found in the intestinal epithelium and can replicate the organ-specific morphology.[8] They also possess a functional stem cell niche and crypt formation.[8] Organoids closely resemble the structure and function of the full organ, making them suitable for studying tissue development and regeneration.[9] Additionally, organoids derived from biopsy-derived intestinal stem cells or induced pluripotent stem cells (iPSCs) can be used to investigate disease-related mechanisms.[10,11] Organoids exhibit a polarized intestinal epithelium when cultured in an extracellular matrix (ECM), with the apical side facing the lumen (apical-in). Furthermore, it is possible to cultivate the organoids in suspension, reversing their polarity, with the apical side being oriented toward the external milieu (apical out).[12] This culture condition closely mimics the in vivo situation

and is particularly useful for infection studies, but is not 100% efficient.[12] However, fragmented organoids, in which the intact spherical structure of the organoids is mechanically disrupted, can also be employed in infection studies and are a simple alternative when a polarized epithelium is not necessary for the specific research question.[10,13]

In a recent study, we could demonstrate that cholesterol levels in Caco-2 cells substantially altered the composition of cholesterol- and sphingolipids-enriched lipid-rafts (LRs) in *S. aureus*-infected Caco-2 cells and impaired the apical sorting of the LRs-associated SI, the main disaccharidase in the intestinal brush border membrane (BBM).[14] Consequently, the reduced expression of SI in BBM was associated with reduced functional capacity of SI lending a mechanistic explanation to the carbohydrate malabsorption and diarrhea commonly manifested during *S. aureus* gastrointestinal infection, as well as in other inflammatory bowel diseases.[14] Nevertheless, the link between *S. aureus* infection and lipid raft alteration is still not very well characterized. Previous findings in our group revealed, that hypoxic conditions distinctly impact host–pathogen interactions, as reduced oxygen level can, for example, downregulate the proper expression of integrin[15] in Caco-2 cells, and inhibit other surface transport proteins.[16] Thus, it might be speculated that oxygen stress is a key modulator during *S. aureus* intestinal infections and its associated molecular alterations.

Therefore, we here investigated *S. aureus* intestinal infection to unravel the molecular and pathophysiological changes including the oxygen level in three different in vitro human models: iPSCs, colonic intestinal stem cell-derived intestinal organoids (colonoids), and Caco-2 cells as a well-established enterocytes model. We also aimed at elucidating the influence of *S. aureus* infection on sterol metabolism and subsequently on intra- and extracellular oxygen levels, as changes of sterol metabolism are often associated with intracellular oxidative stress responses.

2 | MATERIALS AND METHODS

2.1 | Generation of induced pluripotent stem cell (iPSC)-derived intestinal organoids

Human iPSCs, cell line IMR90-4 [WiCell, Madison, Wisconsin, USA],[17] were differentiated to intestinal organoids based on Munera et al.[18] with minor modifications. Standard cultivation of IMR90-4 was conducted in 6-well plates, coated with high-concentrated, growth factor-reduced Matrigel (Corning, New York, USA, #354263) in StemMACS iPS-Brew XF medium (Miltenyi, Bergisch Gladbach, Germany, #130-104-368) supplemented with 100 U/mL penicillin and 100 µg/mL streptomycin [Biochrom, Berlin, Germany, #A0283]. Medium was changed every other day and cells were routinely subcultivated using 0.02% ethylenediaminetetraacetic acid (EDTA) in phosphate-buffered saline without Mg^{2+} and Ca^{2+} (PBS). After passaging 10 µM Rho-Kinase inhibitor Y-27632 (TargetMol, Boston, MA, USA, # T1725) was added to the medium. For differentiation of intestinal organoids (n = 3, three independent differentiations) 100 000 IMR90-4 cells (passage 26 to 34) were seeded per well in 24-well plates (Thermo Scientific, Waltham, Massachusetts, USA, #142485) coated with hESC-qualified Matrigel (Corning, #354277). During differentiation medium was changed every day until D9 (differentiation day 9). On D0 (cell seeding) and D1 StemMACS iPS-Brew XF medium supplemented with 100 U/mL penicillin and 100 µg/mL streptomycin was used with the addition of 10 µM Rho-Kinase inhibitor Y-27632 on D0. From D2 to D4 endoderm differentiation medium with RPMI 1640 (Biochrom, #F1215), 2 mM L-glutamine (Biochrom, #K0283), 100 U/mL penicillin, and 100 µg/mL streptomycin and 1% non-essential amino acids (Biochrom, #K0293) was used. 100 ng/mL Activin A (Miltenyi, #130-115-012) and 15 ng/mL BMP4 (Sigma, #SRP3016) were added to the medium on D2. 100 ng/mL Activin A, 0.2% or 2% heat-inactivated fetal calf serum (FCS) (Biochrom) were added on D3 and D4, respectively. From D5 to D8 mid-hindgut differentiation medium with RPMI 1640, 2 mM L-glutamine, 2% heat-inactivated FCS, 100 U/mL penicillin, and 100 µg/mL streptomycin was supplemented by 500 ng/mL FGF4 (Miltenyi, #130-109-387) and 3 µM CHIR99021 (axon medchem, Groningen, the Netherlands, #Axon 1386). On D9 spheroids were collected from the 24-well plate, pooled and plated in LDEV-free Matrigel (Corning, #354234), which was previously supplemented by 1% B-27 supplement (Thermo Fisher, #12587010) and 100 ng/mL EGF (Biochrom, #1325950100), with a minimum of 50 spheroids per well in a 4-well plate (Thermo Fisher, #176740). Then intestinal growth medium with advanced DMEM/F-12 (Thermo Fisher, #12634010), 1% N2 supplement (Thermo Fisher, #17502048), 2% B-27 supplement, 15 mM HEPES [Biochrom, #L1613], 2 mM L-glutamine, 100 U/mL penicillin, and 100 µg/mL streptomycin was supplemented with 100 ng/mL EGF and 100 ng/mL BMP2 (Miltenyi, #130-110-923) on D9 and only with 100 ng/mL EGF from D12, with medium change every 3–4 days. Medium was changed to 50% intestinal growth medium and 50% long-term culture medium with advanced DMEM/F-12, 2 mM GlutaMAX (Thermo Fisher, #35050061), 50% (v/v) LWRN supernatant (selfmade, according to Ref. [19]), 10 mM HEPES, P/S, 2% B-27 supplement, 50 ng/mL EGF, 1 mM N-acetyl-L-cysteine (Sigma, #A7250), 10 µM Y27632, 500 nM A83-01 (MedChemExpress, New Jersey, USA, #HY-10432), 10 µM SB202190 (MedChemExpress,

#HY-10295), 10 nM gastrin 1 (MedChemExpress, #HY-P1097) according to Ref. [20] on D20. Intestinal organoids were further cultivated according to Ref. [20]. All infection experiments started at D28.

2.2 | Gene expression analysis during differentiation of iPSC to intestinal organoids

Gene expression in iPSCs and intestinal organoids derived thereof was evaluated by RT-qPCR to verify the differentiation status of the cells. In general RNA extraction, reverse transcription and gene of interest expression were performed as previously described.[21] Relative gene expression levels were calculated according to the $2^{-\Delta C}{}_{q}$ method.[22] Random samples of iPSCs and samples taken during intestinal organoid differentiation have been analyzed for expression of the candidate reference genes *ACTB*, *GAPDH*, *PPIA*, *YWHAZ*, *UBC*, *HPRT1*, *B2M*, *RPS23*, and *RPLP0*. Cyclophilin A *(PPIA)* and ribosomal protein S23 (*RPS23)* have been identified to be the most stably expressed reference genes. Expression of stably expressed reference genes has been analyzed with the geNorm algorithm,[23] via qbase+, version 3.0 (Biogazelle, Zwijnaarde, Belgium, www.qbaseplus.com).

The respective primers were used for the detection of genes of interest, associated to be expressed in the specialized intestinal epithelial cells (Table 1). The following genes of interest were analyzed: SRY-Box Transcription Factor 9 (*SOX9*), being baseline expressed in crypt-based columnar stem cells and highly expressed in enteroendocrine cells,[24] leucine-rich repeat-containing G-protein coupled receptor 5 (*LGR5*), an intestinal stem cell marker,[25] lysozyme (*LYZ*), as Paneth cell marker,[26] mucin 2 (*MUC2*), expressed by mucin-producing cells in the whole intestine,[27] as well as chromogranin A (*CHGA*), expressed by enteroendocrine cells.[28]

2.3 | Periodic acid–Schiff (PAS) and immunofluorescence staining

All staining were performed with paraffin-embedded organoids fixed 7 days after passaging by using either 3% paraformaldehyde (PFA), modified Davidson's fluid (mDF) or Bouin solution (Table 2). Periodic acid–Schiff staining was performed on mDF-fixed organoids according to the manufacturer's protocol (Carl Roth, Karlsruhe, Germany) without counterstaining with hemalaun.

For immunofluorescence staining the slides were deparaffinized, permeabilized with Triton X-100 for 60 min and blocked with 5% goat serum in PBS for another 60 min. If necessary, antigen retrieval was performed by heating the slides in citrate buffer at 96–99°C for 20 min after deparaffinization. Primary antibodies to villin (1:50, #M3637, Agilent Technologies, Santa Clara, USA), SOX9 (1:2000, #AB5535 Chemicon International, Temecula, USA) or chromogranin A (CHGA; 1:1000, #20085, Immunostar, Hudson, USA) were added and left overnight at 4°C. The slides were washed with PBS and treated with secondary antibody goat anti-mouse IgG Alexa Fluor® 488 (1:1500, #A11001, Invitrogen, Waltham, USA) or goat anti-rabbit IgG Alexa Fluor® 568 (1:1000, #A11036, Invitrogen) for 45 min. Afterwards, the slides were washed and mounted with ProLong™ Gold Antifade Mountant with DAPI

TABLE 1 Primers used for gene expression quantification.

Genes	Forward primer (5′-3′)	Reverse primer (5′-3′)
PPIA NM_001300981.2	GCCAAGACTGAGTGGTTGGAT	GGCCTCCACAATATTCATGCC
RPS23 NM_001025.5	ACAGGATGGGCAAGTGTCGT	CACTTCTGGTCTCGTCGGTG
SOX9 NM_000346.4	GCTCTGGAGACTTCTGAACGA	CCGTTCTTCACCGACTTCCT
LGR5 NM_001277226.2	CCTTCCAACCTCAGCGTCTT	CCGCAAGACGTAACTCCTCC
LYZ NM_000239.3	AGCCGCTACTGGTGTAATGA	CATGCCACCCATGCTCTAAT
MUC2 NM_002457.4	ATGCCCTTGCGTCCATAACA	AGGAGCAGTGTCCGTCAAAG
CHGA NM_001275.4	AGGAAGAAGGCCCCACTGTA	CGACCGACTCTCGCCTTTC

TABLE 2 Overview of pretreatment, fixatives, and secondary antibodies.

Primary antibody	Fixative	Antigen retrieval	Secondary antibody
SOX9	Bouin	Yes	Goat anti-Rabbit IgG Alexa Fluor® 568
CHGA	PFA	No	Goat anti-Rabbit IgG Alexa Fluor® 568
Villin	Bouin	No	Goat anti-Mouse IgG Alexa Fluor® 488

(#P36941, Thermo Fisher Scientific, Waltham, USA) and imaged with an inverse fluorescence microscope Axiovert 200M (Zeiss, Oberkochen, Germany).

2.4 | Generation of human adult stem cell (aSC)-derived colonoids

Human colonoids were cultivated from crypts obtained from surgically removed colon tissue and grown as previously described.[29] Briefly, the mucosa of the colonic tissue was lifted off the muscle layer and incubated with chelating buffer [10 mM ethylenediaminetetraacetic acid (EDTA) in PBS, pH 8.0] at 4°C for 90 min with shaking. Isolated crypts were washed twice with PBS and 500 crypts each were resuspended in 50 µL growth factor reduced matrigel (Corning) and seeded per well into a pre-warmed 24-well culture dish. After solidification of matrigel at 37°C, 1 mL of organoid growth medium (advanced DMEM/F12) supplemented with 2 mM GlutaMax, 10 mM HEPES, 100 U/mL penicillin, 100 µg/mL streptomycin, B27 supplement (1X, Gibco), 50 ng/mL recombinant EGF (Peprotech), 500 nM A83-01 (Tocris), 10 µM SB202190 (Tocris), 10 nM gastrin I (Tocris), 1 mM *N*-acetyl-L-cysteine (Sigma), and 50% supernatant of L-WRN cells (ATCC® CRL-3276™, containing Wnt3a, R-spondin and Noggin). 10 µM Y27623 (Tocris) was added to the medium on the day of isolation but omitted in subsequent medium exchanges. Use of surgical material was approved by the ethics committee of Hannover Medical School and patients gave their informed consent (approval# 3082-2016).

2.5 | Infection and intracellular presence of *S. aureus* Newman in intestinal organoids

Prior to infection, culture medium was aspirated, and then 1 mL of ice-cold PBS was added to each well containing Matrigel-embedded organoids. To break down the Matrigel and to fragment the organoids, the well contents were pipetted up and down 20 times using a 1000 µL pipet tip, followed by additional 15 times using a 200 µL pipet tip attached to the top of the 1000 µL tip. The organoids were examined under a microscope to ensure efficient fragmentation. Subsequently, the cells were washed with antibiotic-free organoids culture medium. Intestinal cells were counted using the Neubauer counting chamber. As intracellular invasion rate is very low, intestinal organoids were infected with 3.3×10^8 colony forming units (CFU)/mL *S. aureus* Newman (multiplicity of infection (MOI) of 200) in antibiotic-free medium, centrifuged at 140*g* for 5 min to allow contact of cells and bacteria and then incubated under normoxic conditions for 90 min. Intra- and extracellular CFUs were determined using a classical adherence and invasion assays after 90 min incubation with *S. aureus* Newman (T0) as previously described.[14,30] All non-adherent bacteria were washed away with antibiotic-free medium, to determine intracellular bacteria, all extracellular bacteria were killed with 100 µg/mL gentamicin (Sigma, #G-1272). Then, intracellular CFU was determined in trypsinized and lysed cells, as previously described,[14,30] after 1 h (T 1 h), 24 h (T 24 h), and 48 h (T 48 h), the time line is shown in Figure 2A. To determine all adherent plus intracellular bacteria (T 0 h) for comparison and to be able to determine the invasion rate, CFU was also quantified in trypsinized and lysed cells that were not treated with gentamicin, as previously described.[14]

2.6 | Protein concentration over time in intestinal organoids

Organoids were washed twice with PBS after infection and centrifuged at 1000 rcf for 5 min at 4°C. Then, 350 µL of NP-40 buffer (containing 150 mM sodium chloride (Roth, # 9265.1), 1% NP-40 (Thermo Scientific, #85124), 50 mM Tris pH 8.0 (Roth, #5429.1), 5 mM EDTA (Roth, #8043.3)), and 1% protease inhibitor mix (antipain 1.48 mM (#A-6191), pepstatin A 1.46 mM (#P-5318), leupeptin 10.51 mM (#L-8511), aprotinin 0.768 mM (#A-1153), soybean trypsin inhibitor 50 mg/mL (#T-9128), and phenylmethylsulfonyl fluoride (PMSF) 1 mM (#P-7629); all were obtained from Sigma), was added to each sample, frozen in liquid nitrogen and stored at −20°C. After thawing the samples on ice, the organoids were sonicated (Sonoplus rod sonicator; Bandelin) twice for 10 s (10 s with 10 pulses of 0.1 s each and 0.9 s rest in between, at 30%–35% full power of the rod). Between the two sonications, the samples were put on ice for 20 s to avoid overheating. Then, the samples were allowed to cool for 20 min at 4°C and centrifuged at 16000 rcf.

Thereafter, the supernatant was removed, and the pellet discarded. Protein concentration determination was performed by Pierce Microplate BCA Protein Assay Kit-Reducing Agent Compatible (Thermo Scientific, #2352) from the supernatant according to the manufacturer's instructions. The BSA standard was prepared with 0.9% sodium chloride (Carl Roth, #3957.1), 0.05% sodium-azide (Sigma Aldrich, #S-8032), Albumin Fraction V (Carl Roth, #CP84.2) and used in three replicates. Protein concentration determinations were completed in 96-well plates, with 13 µL of each sample dispensed to the bottom of the microplate wells and 260 µL of working reagent added. The plate was covered, mixed thoroughly on a shaker (SIA Biosan, PST-60HL-4, Latvia) for 0.5 min (675 rpm), and incubated at 37°C for 30 min. Finally, the plate was cooled at room temperature for 5 min and absorbance was measured at 562 nm in a plate reader, Infinite M200 (Tecan, Männedorf, Switzerland).

2.7 | Lipid extraction

Samples for lipid extraction were collected 48 h postinfection, from the two organoids models and the Caco2 cells, after the supernatant was removed, and cell pellets were washed with sterile PBS. The samples were centrifuged at 600 rcf and 250 µL trypsin–EDTA was added to detach the cells within 10 to 20 min at 37°C.

Subsequently, 500 µL medium with 100 µg/mL gentamicin was added and the cells resuspended followed by centrifugation at 600 rcf for 5 min. The medium was discarded, the cell pellet washed with PBS (PBS tablet (Medicago, #09-8912-100), and dissolved in 500 mL lipopolysaccharide (LPS)-free water (Roth, #3255)). The supernatant was removed and 100 µL of 5 mg/mL butylhydroxytoluol (BHT) (Sigma, #B1378) and 900 µL HPLC quality water (Carl Roth) were added and the tubes were stored at −20°C. Lipid extraction was performed according to[31] based on the Bligh and Dyer method.[32]

2.8 | Cholesterol and oxysterol analysis by high-performance liquid chromatography (HPLC)

For the cholesterol and oxysterol measurements, a Hitachi Chromaster High-Perfomance Liquid Chromatograph (HPLC) was used with a VDSpher PUR C18-H (3 µm, 150 × 2.0 mm) column (VDS Optilab, Berlin, Germany) as previously described.[31,33] The results were then analyzed and the concentrations were calculated according to the prepared standard. Cholesterol standard was obtained from Sigma (#C8667), from which a standard curve was made (Figure 3A) All oxysterols standards were obtained from Cayman chemicals; 25-hydroxy-cholesterol (25-HC) (#11097), 25(R)-27-hydroxycholesterol (25(R)27-HC) (#14790), 7-keto-cholesterol (7-OC) (#16339), 7β-hydroxycholesterol (7β-HC) (#20099), and 4β-hydroxycholesterol (4β-HC) (#19518).

2.9 | Extracellular oxygen measurement

Caco-2 cells were grown in OxoDish® OD24 plates (PreSens, Regensburg, Germany) until 7 days post confluence. Organoids were mechanically freed from Matrigel by pipetting and centrifuging at 200*g* 5 min. Organoids were resuspended in 0.5 mL antibiotic free medium. Organoid structure was destroyed by pipetting with small filter tip using shear forces as described in Section 2.5. Fragmented organoids were transferred into OxoDish® OD24 plates where they float freely in 0.5 mL cell culture medium per well before and during infection with *S. aureus* and in 1 mL gentamicin-containing medium for 48 h postinfection. Oxygen content of the medium was measured by a SDR SensorDish® Reader (PreSens) at 37°C, 5% CO_2 in water saturated air every 5 min from 30 min before, until 48 h after *S. aureus* infection. Data were processed with PreSens SDR_v4.1.0 software, Excel 2016, and GraphPad Prism 9.0.0 (GraphPad Software, San Diego, California, USA, www.graphpad.com).

2.10 | Intracellular oxygen measurement

Organoids were mechanically freed from Matrigel by pipetting and centrifugation at 200*g* for 5 min. The organoids were resuspended in the amount of antibiotic-free medium corresponding to the number of wells. 0.5 mL per well of the now Matrigel-free organoids were seeded into 24-well plate and provided with the amount of nanobeads (MitoXpress Intra, Agilent Technologies, Santa Clara, CA, USA) indicated by the manufacturer for 24 h to allow the beads to be taken up into the cells. After a washing step to remove unabsorbed nanoparticles, the organoids were mechanically fragmented with a small pipette tip by exploiting shear forces as described in Section 2.5. Intracellular oxygen content was measured in the free-floating organoid fragments by reading the quenching signal in a dual-read time resolved fluorescence measurement using a Tecan Spark plate reader (Tecan) at 37°C, 5% CO_2 according to the manufacturer's instructions. Organoid fragments also float freely in the medium during infection with *S. aureus* (MOI 200). As a result, this shows high standard deviations due to the mobility of the organoids in

the medium, which we tried to mitigate by lightly fixing the cells with Matrigel (Corning, #354234) after changing the medium to gentamicin containing medium to stop the infection. The final results were calculated with Excel 2016 according to the manufacturer's recommendations.

2.11 | Visualization of spatial oxygen distribution with the VisiSens TD system

A two-dimensional optical measurement and mapping of oxygen, sensor foils (SF-RPSu4, PreSens) were cut into squares of 0.49 cm^2 and stuck on the bottom of three wells of a 48-well plate (Greiner, Kremsmünster, Austria, # 677180). Before starting the experiment, a two-point calibration with oxygen-free solution (0% oxygen saturation) and ambient air (100% oxygen saturation) was performed at 37°C, 5% CO_2 in water-saturated air and evaluated with the VisiSens™ ScientifiCal Software v1.0.2.9 (PreSens) according to the manufacturer's protocol. Following disinfection with 70% ethanol, wells with sensor foils were coated with Matrigel as described in Section 2.10.

Fragmented organoids were transferred in 0.5 mL medium to two of the coated wells and the third well was filled with the equivalent volume of medium. Before infection, relative oxygen saturation was measured for 10 min (one shot every 10 s). Then, one well was infected with *S. aureus* Newman as described in Section 2.4 and oxygen saturation was measured for 1 h 15 min (one shot every 3 min). Afterwards, the infection was stopped as described in Section 5 and oxygen was measured for further 48 h (one shot every 10 min), interrupted once by medium exchange after 24 h. Oxygen measurement was performed with the VisiSens TD system (PreSens) at 37°C, 5% CO_2 in water-saturated air. The evaluation of the recordings was carried out with VisiSens™ ScientifiCal Software by choosing a region of interest of 10 × 76 pixels. The oxygen data were converted into figures using Graphpad Prism™ v9.0.0. The single sequences created in the VisiSens™ ScientifiCal Software were combined in Adobe® Premiere® Pro v15.4.1 (Adobe, San José, CA, USA) to a continuous video.

2.12 | Statistical analysis

Experiments were carried out in duplicate or triplicate and repeated in two to three independent experiments as indicated in the figure captions. Statistical analysis of the data was performed in GraphPad Prism 9.

3 | RESULTS

3.1 | iPSC-derived intestinal organoids express marker genes and proteins of specific cells of the intestinal epithelium

To characterize IMR90-4-derived intestinal organoids emphasizing their physiological differentiation, RT-qPCR, histological and immunofluorescence staining of intestinal epithelial cell markers were performed and the polarity of the intact organoids before infection was assessed. RT-qPCR analyses show significantly higher expression of *LGR5*, *SOX9*, *LYZ*, *CHGA*, and *MUC2* in iPSC-derived intestinal organoids compared to iPSCs (Figure 1A). Immunofluorescence staining revealed CHGA- as well as SOX9-positive cells (Figure 1B). Cell membranes facing toward the organoid lumen are villin-positive (Figure 1B). Mucus-producing cells in the organoids were stained with PAS (Figure 1C). Morphologically, the iPSC-derived organoids resemble typical intestinal organoids with crypt-like structures.

The data from RT-qPCR combined with different staining procedures are compatible with a differentiation of iPSCs into intestinal organoids (Figure 1). Similarly, human colonoids display an epithelial crypt structure consisting of differentiated enterocytes, goblet cells, enteroendocrine cells in addition to stem cells and transit amplifying cells.[34]

3.2 | Intracellular survival of *S. aureus* Newman in aSC and iPSC-derived intestinal organoids

To evaluate the existence and the growth of the bacteria inside the organoid cells, the bacteria was cultured to calculate the CFU at three time points (1, 24, and 48 h). The intracellular survival of *S. aureus* Newman in organoids shows that the pathogen was able to enter the cells. However, comparing the percentages of associated or invasive bacteria 1, 24, or 48 h postinfection revealed only subtle differences between the three sampling times (0.4% on average) in the case of iPSC-derived organoids (Figure 2B), while it was reduced by 100% from 25 h to 48 h in the case of colonoids (Figure 2C).

The relative stability of total protein concentrations in both organoid models (Figure 2D,E) suggests that there is a stable cell amount available in infected and noninfected samples. This finding is consistent with previous results in Caco-2 cells.[14]

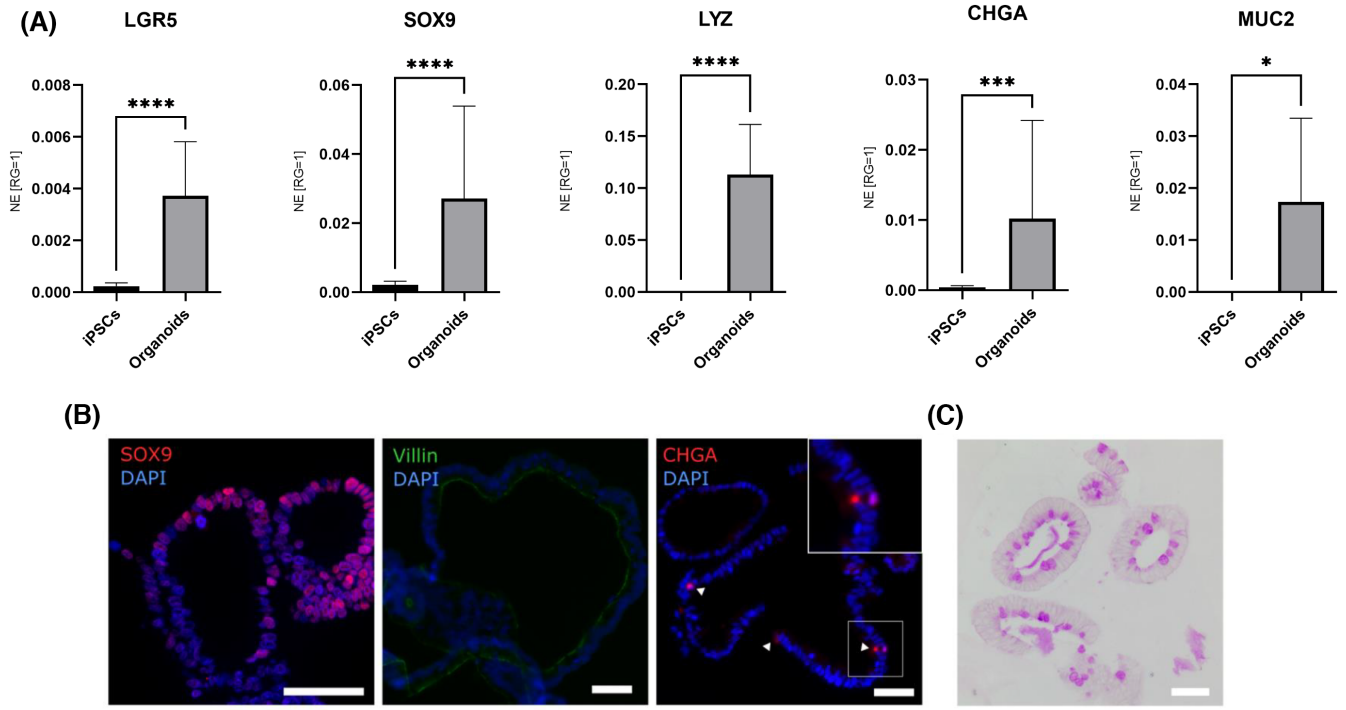

FIGURE 1 Gene expression of LGR5, SOX9, LYZ, CHGA and MUC2 in iPSCs and iPSC-derived intestinal organoids. Immunofluorescence staining and PAS staining in iPSC-derived intestinal organoids. (A) RT-qPCR data shows the expression of intestinal epithelial cell marker genes LGR5 and SOX9 for intestinal stem and progenitor cells, LYZ for Paneth cells, CHGA for enteroendocrine cells and MUC2 for goblet cells in iPSCs and intestinal organoids normalized to reference genes (RG) PPIA and RPS23. $n = 3$, three technical replicates, mean ± standard deviation are shown; Shapiro-Wilk followed by one-tailed Mann-Whitney; as not all the data were normally distributed analyzing residuals, $^{*}p < .05$, $^{***}p < .001$, $^{****}p < .0001$. (B) Immunofluorescence staining of iPSC-derived intestinal organoids. DAPI (blue), SOX9 (red), Villin (green) and CHGA (red) are stained. Scale bar = 50 μm. (C) Periodic acid Schiff staining of iPSC-derived intestinal organoids. Scale bar = 50 μm.

3.3 | Cholesterol content in organoids is significantly reduced after *S. aureus* infection

We have previously shown, that cholesterol sorting and distribution to the surface membrane are significantly altered after *S. aureus* infection and associated with functional alterations in the surface membrane of polarized monolayer cell culture in Caco-2 cells.[14] As 80%–95% of cellular cholesterol is found in the plasma membrane,[35] we analyzed the total cholesterol content in organoids upon infection as a physiological relevant model.

Interestingly, total cholesterol is reduced two-fold in both infected intestinal organoid models (Figure 3B,C) indicating that sterol metabolism might be implicated during this bacterial intestinal infection. Reduced cholesterol levels have been found to disarrange plasma membrane domains, and impact function of membrane proteins, hence resulting in variable physiological alterations as previously shown by others.[36–40]

3.4 | Intracellular and extracellular oxygen levels drop into hypoxic range immediately after *S. aureus* infection

We were interested to scrutinize the intracellular as well as the extracellular oxygen concentration to find out if the recently reported brush border membrane alterations[14] might be related to a hypoxic environment in the cell as previously reported in Caco-2 cells.[15] Immediately after infection with *S. aureus*, a sharp drop in the extracellular oxygen content is seen in the infected organoids (Figure 4A). Even after killing the extracellular bacteria with gentamicin, there is no more alignment with the oxygen contents of the uninfected organoids. Additionally, after changing the medium after 24 h to ensure the supply of nutrients to the cells, the increase in extracellular oxygen content is only brief and drops again below the oxygen level of the uninfected cells. Overall, the oxygen levels of infected and uninfected organs converge over the long experimental period.

Noticeable reduction of oxygen in the media is also reflected inside the cells, as shown in Figure 4B. An

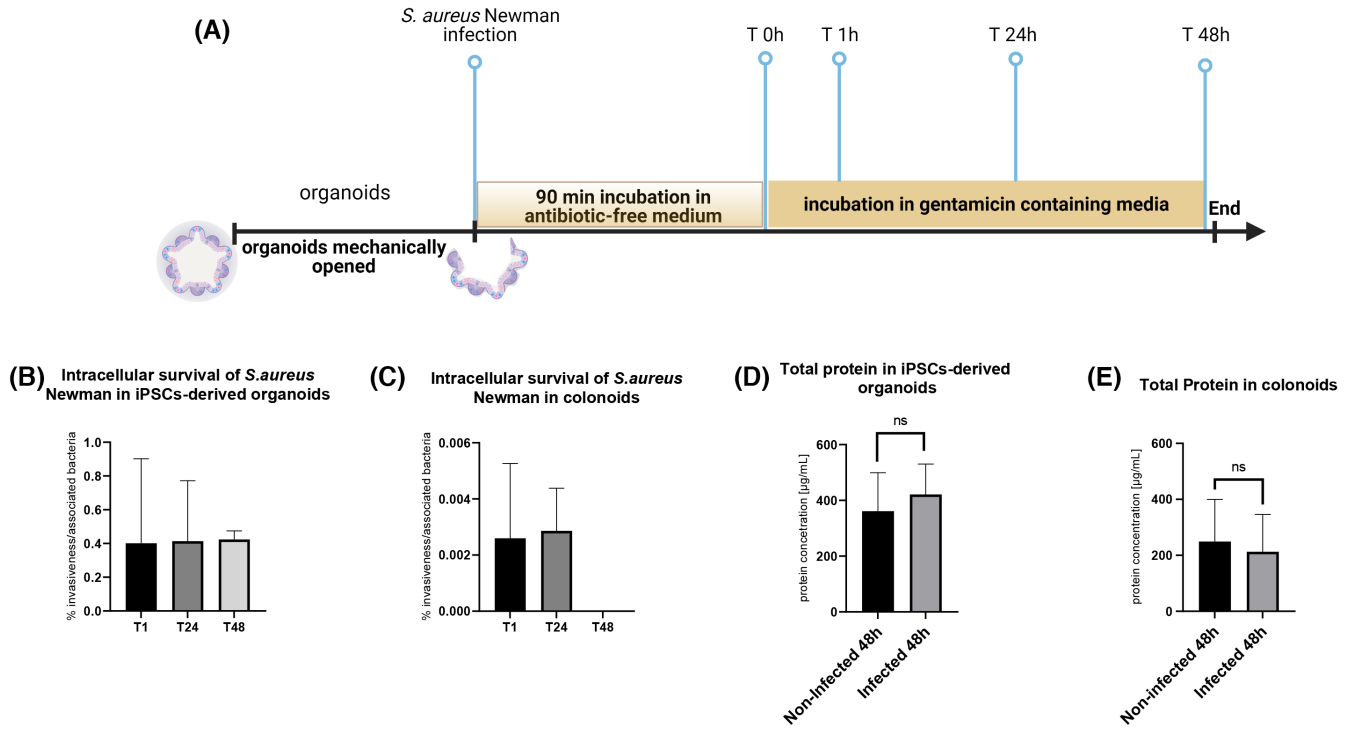

FIGURE 2 A timeline of the experiment plus intracellular survival of *S. aureus* Newman and total protein measurement in intestinal organoids. (A) Timeline of the experiment with infection of organoids (iPSC-derived intestinal organoids and colonoids) and 90 min incubation with subsequent gentamicin treatment and sampling times after one (T 1 h), 24 (T 24 h) and 48 h (T 48 h). (B) and (C) Invasion rate of *S. aureus* Newman in iPSC-derived intestinal organoids and colonoids, respectively, after infection with *S. aureus* Newman (MOI 200) and subsequent gentamicin treatment for one (T1), 24 (T24) and 48 h (T48). The percentage of the CFU inside the cells was calculated in regard to CFU attached to the cells at T0; a Friedman test was applied, mean values with SD of $n = 3$. Total protein measurement of infected and uninfected iPSC-derived intestinal organoids (D) and colonoids (E) after 48 h incubation. Shapiro-Wilk followed by one tailed Mann-Whitney was used, as not all the data were normally distributed. Mean values with SD± of $n = 3$, ns = non-significant.

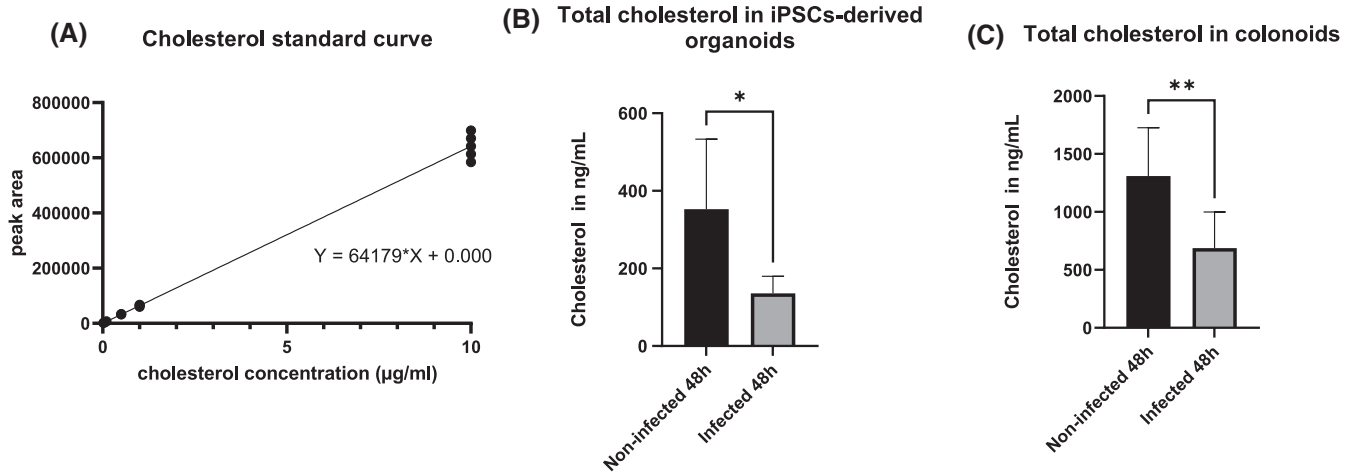

FIGURE 3 More than two-fold reduction in total cellular cholesterol in intestinal organoids due to infection. (A) Standard curve for quantification of the detected cholesterol amount ($n = 5$) the concentration ranged between 10 µg/mL and 0.01 µg/mL with a limit of detection of 20 ng/mL in the tested samples. The total amount of cholesterol in iPSC-derived intestinal organoids (B) and colonoids (C) 48 h after infection with *S. aureus* Newman at MOI 200 compared to non-infected cells. Significant reduction of cholesterol concentration in ng/mL in each plate's well. *$p \leq .05$, **$p \leq .01$ by using one-tailed Student's *t*-test after confirming normal distribution of the data by Shapiro-Wilk test. Data represent mean values with SD± of $n = 3$.

immediate drop in intracellular oxygen content occurs with the onset of *S. aureus* infection. The intracellular oxygen content drops faster than the extracellular oxygen content, so that it cannot be assumed that the intracellular oxygen content adjusts to the extracellular one.

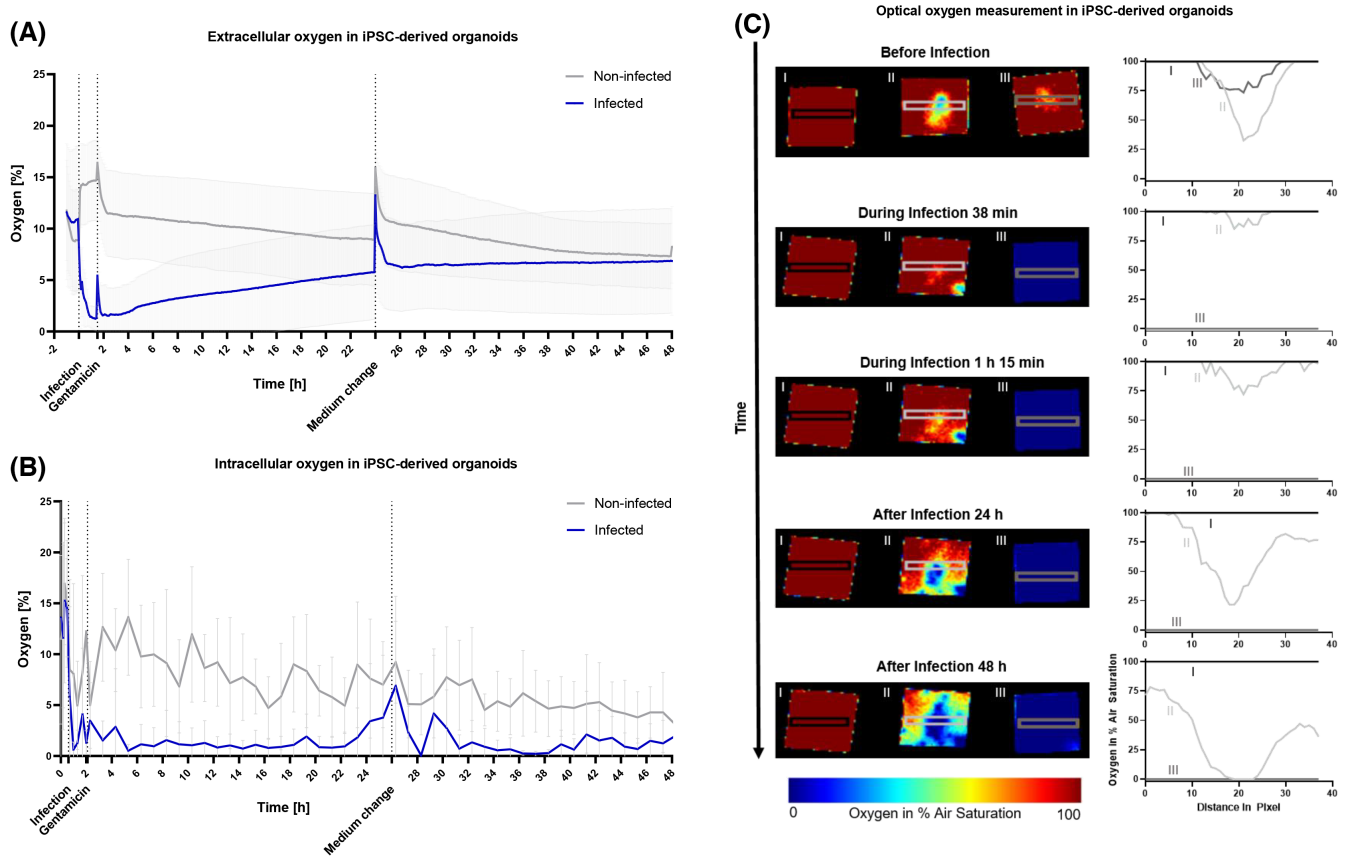

FIGURE 4 Oxygen measurement in iPSC-derived intestinal organoids. (A) Measurement of extracellular oxygen using non-oxygen consuming fluorescence based oxygen measurement with SDR reader (PreSens). Upon *S. aureus* infection (MOI 200), the oxygen content in the medium drops more than in that of uninfected organoids. Medium change inserts oxygen in the system. Throughout the experimental period, the extracellular oxygen content in infected organoids is lower than in uninfected organoids but the values converge over 48 h. Mean values with SD of $n = 3$. (B) Measurement of intracellular oxygen. Immediately after *S. aureus* infection, oxygen decreases more in infected organoids than in uninfected organoids. Medium change inserts oxygen in the system and also increases the intracellular oxygen content. To avoid movement and therefore disturbance of the measurement the organoids were fixed to the well bottom with Matrigel®. Throughout the following experimental period, the intracellular oxygen content in infected organoids is lower than in uninfected organoids. Mean values with SD of $n = 3$. O_2-sensitive cell-penetrating nanoparticles (Agilent MitoXpress intra) were measured inTecan Spark. Dual-read time resolved fluorescence measurement with excitation at 380 nm and emission at 670 nm. Incubation 37°C 5% CO_2. (C) Spatial oxygen distribution of non-infected (II) and infected (III) organoids or medium alone (I). Pictures were taken at 5 different timepoints using VisiSens TD system (PreSens). Graphs indicate the oxygen levels at the respective positions inside the corresponding rectangles (10×76 pixels) of the accompanying images. One hundred percent air saturation corresponds to the oxygen value of the air in the incubator at which the system was calibrated.

Furthermore, the optical measurement of oxygen distribution of infected and uninfected iPSC-derived organoids (Figure 4C) with a system using sensor foil shows similar results to the intracellular oxygen measurement (Figure 4B). After infection of organoids, the well becomes hypoxic throughout, which is stable until the end of the experiment. Measuring the uninfected organoids showed hypoxic areas, which continuously decreases in oxygenation and expands slowly over the course of time. During the whole measurement, the oxygen values of the uninfected organoids are higher than the levels of the infected.

In colonoids (Figure 5A), there is again an instant reduction in oxygen content in the medium after *S. aureus* infection (MOI 200). Medium change introduced oxygen in the system. Unlike the iPSC derived organoids, the extracellular oxygen remains below 1% without tendency to reraise gradually during infection. Similarly, the intracellular oxygen content (Figure 5B) in infected colonoids is lower than in uninfected colonoids. Fresh medium change barely increases the intracellular oxygen content. Throughout the experimental period, the intracellular and extracellular oxygen content in infected cells is lower than in uninfected cells.

4 | DISCUSSION

Animal models, most often mouse models, provide an effective way to study host–pathogen interactions at

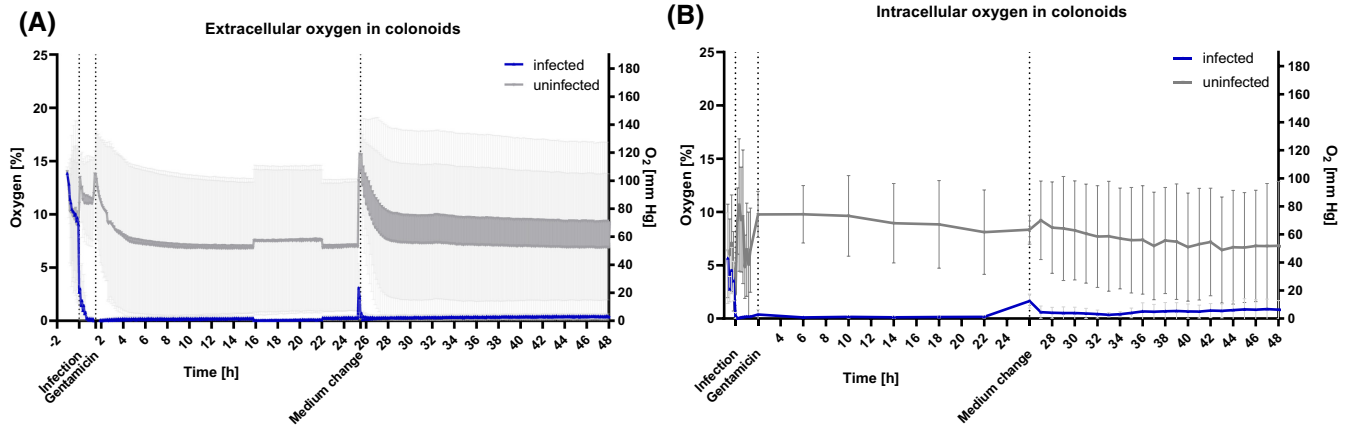

FIGURE 5 Oxygen measurement colonoids. To avoid movement and therefore disturbance of the measurement the organoids were fixed to the well bottom with Matrigel®. (A) Measurement of extracellular oxygen: Non-oxygen consuming fluorescence-based oxygen measurement was performed with SDR reader (PreSens). Mean values with SD of $n = 3$. (B) Measurement of intracellular oxygen, shortly after *S. aureus* infection. O_2-sensitive cell-penetrating nanoparticles (Agilent MitoXpress intra) were measured in Tecan Spark. Dual-read time resolved fluorescence measurement with extension and 380 nm and emission at 670 nm. Incubation 37°C 5% CO_2. Mean values with SD of $n = 3$.

the intestinal epithelium, including all specialized cell types, considering regional subdivision of the intestinal segments, the microbiome as well as interaction with the immune system. However, species-specific aspects of infection further need extrapolation, which imposes challenges concerning bacterial tropism and implicated molecular mechanisms. Organoids appear to be promising models in gastroenterology mainly because of constituting a forward step that can replace invasive approaches, such as taking biopsy specimens. In addition, variety of different epithelial cell types in organoids render this model more suitable to resemble the in vivo situation than intestinal cell lines.[9] Nevertheless, many factors and variables need to be standardized to make organoids a suitable alternative to the extensively used monolayer cell culture.

Before exploiting the organoids as a model to study intestinal infection it was essential to first evaluate their physiological differentiation state, therefore iPSC-derived intestinal organoids were initially analyzed for transcription and protein expression of intestinal epithelial differentiation markers. Higher expression of *LGR5* and *SOX9* indicate the presence of intestinal progenitor and stem cells which can also be seen in immunofluorescence staining for SOX9.[24] Higher RNA-expression of *CHGA* can also be shown in immunofluorescence staining and indicates a physiological-like presence of enteroendocrine cells, which make up about 1% of the intestinal epithelium.[41] Increased expression of *MUC2*, together with the finding of PAS-positive cells, indicates a population of goblet cells forming a mucus layer in the organoid lumen.[9] Staining for villin indicates that cells with the apical cell membranes are oriented toward the lumen of the organoids, supporting the in vivo-like polarity of the intestinal epithelium in the organoids.[9] Similarly, the aSC organoids has been found previously to show comparable expression profile to human intestinal epithelium.[29] Following the demonstration of the differentiation and expression status of the two organoid models we proceeded to utilize them as a model for *S. aureus* infection as a more complex as well as physiological or in vivo relevant in vitro method compared to Caco-2-cells, which were previously used by our group.[14]

In all models, the infectivity could highly influence the results. Although both organoid models in this study were infected with 200 MOI with the goal to receive similar infectivity, nevertheless the results of previous studies, for example,[14] could not be observed. Additionally, the intracellular survival rates in the aforementioned study were much higher in Caco-2 cells, suggesting that the Caco-2 cells are more susceptible to infection. Thus, detailed analysis of molecular alterations in the different models are required for its characterization. Because several structural and functional membrane components of Caco-2 cells as well as the cholesterol contents in LRs were altered after *S. aureus* infection in Caco-2 cells,[14] we found it compelling to track cholesterol concentration to reveal the extent of these alterations on the total cellular cholesterol content in the organoids models together with the Caco-2 cells. Although the reduction in total cholesterol was prominent in both organoid models, surprisingly, total cholesterol was not significantly altered in Caco-2 cells (Figure S1A). Differences in the models might be caused by other cell types being expressed in the stem cell-derived intestinal organoid models, the building crypts and an active stem cell niche, which should be investigated in depth in

follow-up studies that focus on infection of the involved cell types. In accordance with this, earlier findings have revealed that certain intestinal pathogens have the ability to impact different intestinal epithelial cells in diverse ways.[42]

Hypoxic conditions in infected tissue environment have been frequently described and attributed not only to the infiltrating immune cells, but also to the invasive microorganisms. Lower oxygen conditions encourage *S. aureus* to transform to fermentative metabolism[43] and replicate while the host cells face unfavorable conditions. Furthermore, this metabolic shift also results in antibiotic resistance[44] making infection inextricable to eradicate. Reduced oxygen condition can also limit the NADPH oxidase and therefore compromise pathogen killing by phagocytes.[45]

On the other hand, hypoxic conditions in enterocytes have been found to alter the association of integrin with LRs and thus reduce the intracellular invasion of bacteria that need these receptors for cell entry.[46] *S. aureus* exploits the apical membrane and integrin to invade the intestinal cells, particularly *S. aureus* Newman strain, which does not bind to fibronectin as an alternative receptor.[47] Therefore, the hypoxic conditions can protect the cells from further attachment of invasive bacteria to the cells and can also lead to more immune cells recruitment through hypoxia inducible factor (HIF)-dependent inflammatory response activation.

Over the time, the hypoxic state of infected organoids did not change after killing the extracellular bacteria with gentamicin and oxygenation remained well below the intracellular oxygen content of uninfected organoids for the entire 48 h experimental period. This finding is supported by Lone et al.[48] where the hypoxic level in skin tissue infected with *S. aureus* in an ex vivo experiment was observed.

A similar severe reduction in oxygen content in an in vivo model has been previously reported but was mainly attributed to infiltration of immune cells.[49] We previously found that exposure to low pO_2 (20–40 mmHg) for 1 h was enough to reflect explicitly HIF-1α expression in Caco-2 cells.[50]

Differences, especially in extracellular O_2, between uninfected iPSC-derived organoids and the uninfected colonoids can also be attributed to physiological variations in oxygen content. It has been previously found that the physiological pO_2 in the colon lumen is 3 mmHg (~0.4% O_2),[51] while in the villus tip and the lumen of the small intestine has been found to be 33 mmHg (~3% O_2) and <10 mmHg (~2% O_2), respectively.[52]

The high standard deviations between the iPSC-derived organoids and the colonoids in extracellular oxygen level compared to the experiments with Caco-2 cells (see Figure S1A) may be explained by the free swimming of the organoids in the wells, which makes them move closer or further away from the sensors.

Our parallel experiments with Caco-2 cells for measuring oxygen, similar to the organoid models, showed a clear reduction in oxygen in infected cells (Figure S1B,C). These findings also suggest that the previously reported alterations in LRs in *S. aureus* infected Caco-2 cells might be a response to the altered oxygen content of the cells. This is also reported for lung tissues, where cholesterol-rich areas of the membrane were suggested to react to control the oxygen diffusion.[53] Our findings in Caco-2 cells also are in line with previous results,[54] which showed that 18 h exposure to hypoxia does not result in alteration in total cholesterol level of primary epithelial monolayer cells.

Because total cholesterol content was different in the organoids and Caco-2 cells, the next question we addressed was whether the sterol metabolism was altered. Therefore, we investigated oxysterols upon *S. aureus* infection, simultaneously with cholesterol. As in the results for total cholesterol, significant alteration in some oxysterols were detected only in the two *S. aureus* infected intestinal organoid models (Figure S1B,C) but not in the Caco-2 cells (Figure S1A). For this, five different oxysterols were detected and measured in both experimental models, namely 25-hydroxy-cholesterol (25-HC), 25(R)-27-hydroxy-cholesterol (25(R)27-HC), 7-keto-cholesterol (7-OC), 7β-hydroxy-cholesterol (7β-HC), and 4β-hydroxy-cholesterol (4β-HC).

Some previous findings claimed that some oxysterols (i.e., 25-hydroxycholesterol) can inhibit the activation of HIF-1α under hypoxic conditions in cardiomyocytes.[55] Therefore, further research must be conducted to determine if these hypoxic conditions are sufficient to activate the hypoxic reaction pathway, orchestrated by HIF transcription.

Effect of oxysterols on bacterial infection has not yet been sufficiently studied and understood. Therefore, significantly altered oxysterols in iPSC-derived organoids and colonoids but not in Caco-2 cells, with higher susceptibility for infection reported earlier,[14] may speculate on their antibacterial effect in limiting bacterial infection as innate defense mediators.

Our results support the previously known role of elevated side-chain oxysterols in reducing cholesterol synthesis through negative feedback to the *SREBPs* (sterol regulatory element binding proteins) transcription factor pathway.[56]

Moreover those oxysterols have a paracrine and autocrine effect in reducing the accessible cholesterol in the surface membrane, that is used by different bacteria to enter and spread between the cells[56,57] and hence

introduce these oxysterols as active elements in the cellular innate defense against pathogens.

Similar implication of side-chain oxysterols has also been previously reported during hypoxic microenvironment conditions, as has been demonstrated in immune cells[58] and the brain.[59]

Conversely, the significant reduction of 25(R)27-HC in colonoids in contrast to its increase in infected Caco-2 cells or in iPSC-derived organoids, might explain the reduced infection rate in colonoids in this study. In fact, 27-HC oxysterols have been found to be important in the formation of endosomes, which is used by many bacteria to survive inside the cell[60] and hence would confer a replication niche to the *S. aureus* Newman, as a vacuolar proliferating pathogen.[61]

The synthesis cascade of cholesterol and oxysterols (Figure S3) shows that ring oxysterols can retard the final step of cholesterol and the subsequent side-chain oxysterol synthesis as the 7-OC can be formed from the cholesterol precursor; 7-dehydrocholestrol.[62] Based on the extreme hypoxic conditions in infected colonoids, lipid isolation under inert gas conditions, and the incorporation of antioxidants in this study, the results suggest a preference of enzymatic formation of 7β-HC from the 7-OC via the antioxidative route from cholesterol. This might also explain the significant reduction of cholesterol and side-chain oxysterols in infected colonoids in favor of ring oxysterols, as reported during colitis.[63]

Rydberg et al., proposed elevated oxysterol levels during hypoxia as a mechanism to activate immune cells through IL-8.[58] In addition we have previously shown that hypoxia was clearly implicated in LRs alteration upon other bacterial infection in Caco-2 cells,[6] and as we were also able to show both these manifestations, we addressed the states of oxygen concentration before and after infection and compared it in the three experimental models. The results from cholesterol and oxysterols in all experimental models suggest that oxysterols play an important role in *S. aureus* Newman infection pathogenesis, subsequent hypoxia, and cholesterol metabolism alterations.

5 | CONCLUSION

Finding reliable models that closely represent the physiological conditions in humans, to study intestinal infections has always been controversial. Recently, the urgent need to find animal alternatives has introduced intestinal organoids as a step further than classic monolayer enterocyte culture, including more physiologically relevant cell types of the intestinal epithelium and morphological similarities to the in vivo intestine. In this study we aimed to determine how far these models can help reveal the molecular mechanisms behind bacterial infections of the intestinal epithelium with a focus on cholesterol content and oxygen level.

Regardless of the phenotypic differences, all tested models showed rapid and long-lasting reduction in oxygen content inside epithelial cells and their ambient environment due to *S. aureus* invasion and intracellular survival.

Although sterol metabolism and lipid rafts have previously been found to play an important role in intestinal infections, few studies have been performed to investigate their pathophysiological influence. The results of this study strongly suggest that membrane alterations originate from cholesterol reduction. Oxysterols, as rapid membrane-crossing messenger within and between cells, might play an important role in the underlying mechanisms that control symptom development and the recruitment of the immune response. The variability between the different models in infection rates and lipid metabolites largely reflects the diversity in differentiation and cellular composition of the models. This can be utilized to understand the variety in possible pathophysiological pathways between individual patients and between different intestinal compartments.

The hypoxic state could affect overall cellular metabolism, which may manifest as impaired lipid metabolism. This in turn influences the epithelial surface membrane structure and functions, to which the irritable bowel symptoms accompanied with *S. aureus* infections of the intestine can be attributed.

AUTHOR CONTRIBUTIONS

Conceptualization: AhmedElmontaser Mergani, Maren von Köckritz-Blickwede, and Bettina Seeger. *Funding acquisition*: Guntram A. Grassl, Maren von Köckritz-Blickwede, and Bettina Seeger. *Investigation*: AhmedElmontaser Mergani, Marita Meurer, Elena Wiebe, Katrin Dümmer, Katrin Wirz, Judith Lehmann, Maren Schenke, and Katrin Künnemann. *Methodology*: Katrin Dümmer, Katrin Wirz, Judith Lehmann, Maren Schenke, Graham Brogden, AhmedElmontaser Mergani, Marita Meurer, Elena Wiebe, Katrin Künnemann, Guntram A. Grassl, Maren von Köckritz-Blickwede, and Bettina Seeger. *Project administration*: Bettina Seeger and Maren von Köckritz-Blickwede. *Resources*: Guntram A. Grassl, Hassan Y. Naim, Maren von Köckritz-Blickwede, and Bettina Seeger. *Supervision*: Maren von Köckritz-Blickwede and Bettina Seeger. *Validation*: AhmedElmontaser Mergani, Marita Meurer, Graham Brogden, Maren von Köckritz-Blickwede, and Bettina Seeger. *Visualization*: AhmedElmontaser Mergani, Marita Meurer, Katrin Dümmer, Katrin Wirz, Maren von Köckritz-Blickwede, and Bettina Seeger.

Roles/writing—original draft: AhmedElmontaser Mergani, Maren von Köckritz-Blickwede, and Bettina Seeger. *Writing—review and editing*: All authors.

ACKNOWLEDGMENTS

The authors thank Jutta Barras-Akhnoukh, Alexander Krybus, Beate Prieß, and Karola Schlote for excellent technical assistance. Open Access funding enabled and organized by Projekt DEAL.

FUNDING INFORMATION

This work was supported by the Federal State of Lower Saxony in the Joint project R2N—"Replace" and "Reduce" in Niedersachsen (Lower Saxony)—Alternative methods to replace or reduce animal models in biomedical research [projects A2 and T3, 74ZN1574] and by MikroReplaceSystems projects P02 and P07 funded by the programme "Zukunft Niedersachsen" of the Federal State of Lower Saxony.

DISCLOSURES

The data that support the findings of this study are available in the methods and/or supplementary material of this article.

DATA AVAILABILITY STATEMENT

The data that support the findings of this study are available in the methods and/or supplementary material of this article.

ORCID

AhmedElmontaser Mergani https://orcid.org/0000-0003-1662-2421
Marita Meurer https://orcid.org/0000-0001-9409-4922
Katrin Wirz https://orcid.org/0009-0002-1840-0363
Maren Schenke https://orcid.org/0000-0001-5649-591X
Hassan Y. Naim https://orcid.org/0000-0003-4884-8425
Guntram A. Grassl https://orcid.org/0000-0003-3718-2090
Maren von Köckritz-Blickwede https://orcid.org/0000-0001-7712-9767
Bettina Seeger https://orcid.org/0000-0002-4653-2841

REFERENCES

1. Holden MT, Feil EJ, Lindsay JA, et al. Complete genomes of two clinical *Staphylococcus aureus* strains: evidence for the rapid evolution of virulence and drug resistance. *Proc Natl Acad Sci U S A*. 2004;101(26):9786-9791.
2. Lowy FD. *Staphylococcus aureus* infections. *N Engl J Med*. 1998;339(8):520-532.
3. Plata K, Rosato AE, Wegrzyn G. *Staphylococcus aureus* as an infectious agent: overview of biochemistry and molecular genetics of its pathogenicity. *Acta Biochim Pol*. 2009;56(4):597-612.
4. Doyle MP, Erickson MC. Reducing the carriage of foodborne pathogens in livestock and poultry. *Poult Sci*. 2006;85(6):960-973.
5. Larcombe S, Jiang JH, Hutton ML, Abud HE, Peleg AY, Lyras D. A mouse model of *Staphylococcus aureus* small intestinal infection. *J Med Microbiol*. 2020;69(2):290-297.
6. Sambuy Y, de Angelis I, Ranaldi G, Scarino ML, Stammati A, Zucco F. The Caco-2 cell line as a model of the intestinal barrier: influence of cell and culture-related factors on Caco-2 cell functional characteristics. *Cell Biol Toxicol*. 2005;21(1):1-26.
7. Aguilar C, Alves da Silva M, Saraiva M, Neyazi M, Olsson IAS, Bartfeld S. Organoids as host models for infection biology—a review of methods. *Exp Mol Med*. 2021;53(10):1471-1482.
8. Rahman S, Ghiboub M, Donkers JM, et al. The progress of intestinal epithelial models from cell lines to gut-on-Chip. *Int J Mol Sci*. 2021;22:13472.
9. Sato T, Vries RG, Snippert HJ, et al. Single Lgr5 stem cells build crypt-villus structures in vitro without a mesenchymal niche. *Nature*. 2009;459(7244):262-265.
10. Co JY, Margalef-Català M, Monack DM, Amieva MR. Controlling the polarity of human gastrointestinal organoids to investigate epithelial biology and infectious diseases. *Nat Protoc*. 2021;16:5171-5192.
11. Günther C, Winner B, Neurath MF, Stappenbeck TS. Organoids in gastrointestinal diseases: from experimental models to clinical translation. *Gut*. 2022;71(9):1892-1908.
12. Co JY, Margalef-Català M, Li X, et al. Controlling epithelial polarity: a human enteroid model for host-pathogen interactions. *Cell Rep*. 2019;26(9):2509-2520 e4.
13. Dutta D, Clevers H. Organoid culture systems to study host–pathogen interactions. *Curr Opin Immunol*. 2017;48(Supplement C):15-22.
14. Mergani A, Wanes D, Schecker N, Branitzki-Heinemann K, Naim HY, von Köckritz-Blickwede M. *Staphylococcus aureus* infection influences the function of intestinal cells by altering the lipid raft-dependent sorting of sucrase-isomaltase. *Front Cell Dev Biol*. 2021;9:699970.
15. Zeitouni NE, Dersch P, Naim HY, von Köckritz-Blickwede M. Hypoxia decreases invasin-mediated *Yersinia enterocolitica* internalization into Caco-2 cells. *PloS One*. 2016;11(1):e0146103.
16. Bourseau-Guilmain E, Menard JA, Lindqvist E, et al. Hypoxia regulates global membrane protein endocytosis through caveolin-1 in cancer cells. *Nat Commun*. 2016;7:11371.
17. Yu J, Vodyanik MA, Smuga-Otto K, et al. Induced pluripotent stem cell lines derived from human somatic cells. *Science*. 2007;318(5858):1917-1920.
18. Munera JO, Wells JM. Generation of gastrointestinal organoids from human pluripotent stem cells. *Methods Mol Biol*. 2017;1597:167-177.
19. Miyoshi H, Ajima R, Luo CT, Yamaguchi TP, Stappenbeck TS. Wnt5a potentiates TGF-β signaling to promote colonic crypt regeneration after tissue injury. *Science*. 2012;338(6103):108-113.
20. Hoffmann P, Schnepel N, Langeheine M, et al. Intestinal organoid-based 2D monolayers mimic physiological and pathophysiological properties of the pig intestine. *PloS One*. 2021;16(8):e0256143.
21. Schenke M, Schjeide BM, Püschel GP, Seeger B. Analysis of motor neurons differentiated from human induced pluripotent stem cells for the use in cell-based botulinum neurotoxin activity assays. *Toxins (Basel)*. 2020;12(5):276.

22. Schmittgen TD, Livak KJ. Analyzing real-time PCR data by the comparative C(T) method. *Nat Protoc*. 2008;3(6):1101-1108.
23. Vandesompele J, de Preter K, Pattyn F, et al. Accurate normalization of real-time quantitative RT-PCR data by geometric averaging of multiple internal control genes. *Genome Biol*. 2002;3(7):Research0034.
24. Formeister EJ, Sionas AL, Lorance DK, Barkley CL, Lee GH, Magness ST. Distinct SOX9 levels differentially mark stem/progenitor populations and enteroendocrine cells of the small intestine epithelium. *Am J Physiol Gastrointest Liver Physiol*. 2009;296(5):G1108-18.
25. Barker N, van Es JH, Kuipers J, et al. Identification of stem cells in small intestine and colon by marker gene Lgr5. *Nature*. 2007;449(7165):1003-1007.
26. Clevers HC, Bevins CL. Paneth cells: maestros of the small intestinal crypts. *Annu Rev Physiol*. 2013;75:289-311.
27. Birchenough GM, Johansson ME, Gustafsson JK, Bergström JH, Hansson GC. New developments in goblet cell mucus secretion and function. *Mucosal Immunol*. 2015;8(4):712-719.
28. Spence JR, Mayhew CN, Rankin SA, et al. Directed differentiation of human pluripotent stem cells into intestinal tissue in vitro. *Nature*. 2011;470(7332):105-109.
29. Schottelndreier D, Seeger K, Grassl GA, Winny MR, Lindner R, Genth H. Expression and (lacking) internalization of the cell surface receptors of Clostridioides difficile toxin B. *Front Microbiol*. 2018;9:1483.
30. Dziewanowska K, Patti JM, Deobald CF, Bayles KW, Trumble WR, Bohach GA. Fibronectin binding protein and host cell tyrosine kinase are required for internalization of *Staphylococcus aureus* by epithelial cells. *Infect Immun*. 1999;67(9):4673-4678.
31. Beck A, Jordan LK, Herlitze S, et al. Quantification of sterols from carp cell lines by using HPLC-MS. *Sep Sci Plus*. 2018;1(1):11-21.
32. Bligh EG, Dyer WJ. A rapid method of total lipid extraction and purification. *Can J Biochem Physiol*. 1959;37(8):911-917.
33. Branitzki-Heinemann K, Brogden G, von Kockritz-Blickwede M. Influence of oxygen on function and cholesterol composition of murine bone marrow-derived neutrophils. *Methods Mol Biol*. 2020;2087:223-233.
34. Boyle EC, Wunschel EJ, Grassl GA. *Salmonella enterica* infection of human and mouse colon organoid-derived monolayers. *Methods Mol Biol*. 2022;2427:149-163.
35. Lange Y, Ramos BV. Analysis of the distribution of cholesterol in the intact cell. *J Biol Chem*. 1983;258(24):15130-15134.
36. Sheets ED, Holowka D, Baird B. Critical role for cholesterol in Lyn-mediated tyrosine phosphorylation of FcepsilonRI and their association with detergent-resistant membranes. *J Cell Biol*. 1999;145(4):877-887.
37. Monastyrskaya K, Hostettler A, Buergi S, Draeger A. The NK1 receptor localizes to the plasma membrane microdomains, and its activation is dependent on lipid raft integrity. *J Biol Chem*. 2005;280(8):7135-7146.
38. Hunter I, Nixon GF. Spatial compartmentalization of tumor necrosis factor (TNF) receptor 1-dependent signaling pathways in human airway smooth muscle cells. Lipid rafts are essential for TNF-alpha-mediated activation of RhoA but dispensable for the activation of the NF-kappaB and MAPK pathways. *J Biol Chem*. 2006;281(45):34705-34715.
39. Suzuki KG, Fujiwara TK, Edidin M, Kusumi A. Dynamic recruitment of phospholipase C gamma at transiently immobilized GPI-anchored receptor clusters induces IP3-Ca^{2+} signaling: single-molecule tracking study 2. *J Cell Biol*. 2007;177(4):731-742.
40. Xu S, Huo J, Gunawan M, Su IH, Lam KP. Activated dectin-1 localizes to lipid raft microdomains for signaling and activation of phagocytosis and cytokine production in dendritic cells. *J Biol Chem*. 2009;284(33):22005-22011.
41. Gunawardene AR, Corfe BM, Staton CA. Classification and functions of enteroendocrine cells of the lower gastrointestinal tract. *Int J Exp Pathol*. 2011;92(4):219-231.
42. Hopkins EGD, Roumeliotis TI, Mullineaux-Sanders C, Choudhary JS, Frankel G. Intestinal epithelial cells and the microbiome undergo swift reprogramming at the inception of colonic *Citrobacter rodentium* infection. *mBio*. 2019;10(2):e00062-19.
43. Xu Y, Maltesen RG, Larsen LH, et al. In vivo gene expression in a *Staphylococcus aureus* prosthetic joint infection characterized by RNA sequencing and metabolomics: a pilot study. *BMC Microbiol*. 2016;16:80.
44. Gupta S, Laskar N, Kadouri DE. Evaluating the effect of oxygen concentrations on antibiotic sensitivity, growth, and biofilm formation of human pathogens. *Microbiol Insights*. 2016;9:37-46.
45. McGovern NN, Cowburn AS, Porter L, et al. Hypoxia selectively inhibits respiratory burst activity and killing of *Staphylococcus aureus* in human neutrophils. *J Immunol*. 2011;186(1):453-463.
46. Zeitouni NE, Chotikatum S, von Köckritz-Blickwede M, Naim HY. The impact of hypoxia on intestinal epithelial cell functions: consequences for invasion by bacterial pathogens. *Mol Cell Pediatr*. 2016;3(1):14.
47. Grundmeier M, Hussain M, Becker P, Heilmann C, Peters G, Sinha B. Truncation of fibronectin-binding proteins in Staphylococcus aureus strain Newman leads to deficient adherence and host cell invasion due to loss of the cell wall anchor function. *Infect Immun*. 2004;72(12):7155-7163.
48. Lone AG, Atci E, Renslow R, et al. *Staphylococcus aureus* induces hypoxia and cellular damage in porcine dermal explants. *Infect Immun*. 2015;83(6):2531-2541.
49. Melican K, Boekel J, Månsson LE, et al. Bacterial infection-mediated mucosal signalling induces local renal ischaemia as a defence against sepsis. *Cell Microbiol*. 2008;10(10):1987-1998.
50. Zeitouni NE, Fandrey J, Naim HY, von Köckritz-Blickwede M. Measuring oxygen levels in Caco-2 cultures. *Hypoxia (Auckl)*. 2015;3:53-66.
51. He G, Shankar RA, Chzhan M, Samouilov A, Kuppusamy P, Zweier JL. Noninvasive measurement of anatomic structure and intraluminal oxygenation in the gastrointestinal tract of living mice with spatial and spectral EPR imaging. *Proc Natl Acad Sci U S A*. 1999;96(8):4586-4591.
52. Fisher EM, Khan M, Salisbury R, Kuppusamy P. Noninvasive monitoring of small intestinal oxygen in a rat model of chronic mesenteric ischemia. *Cell Biochem Biophys*. 2013;67(2):451-459.
53. Zuniga-Hertz JP, Patel HH. The evolution of cholesterol-rich membrane in oxygen adaption: the respiratory system as a model. *Front Physiol*. 2019;10:1340.
54. Ledoux S, Runembert I, Koumanov K, Michel JB, Trugnan G, Friedlander G. Hypoxia enhances Ecto-5′-Nucleotidase activity and cell surface expression in endothelial cells: role of membrane lipids. *Circ Res*. 2003;92(8):848-855.
55. Lappano R, Recchia AG, de Francesco EM, et al. The cholesterol metabolite 25-hydroxycholesterol activates estrogen receptor

α-mediated signaling in cancer cells and in cardiomyocytes. *PloS One*. 2011;6(1):e16631.
56. Griffiths WJ, Wang Y. Cholesterol metabolism: from lipidomics to immunology. *J Lipid Res*. 2022;63(2):100165.
57. Abrams ME, Johnson KA, Perelman SS, et al. Oxysterols provide innate immunity to bacterial infection by mobilizing cell surface accessible cholesterol. *Nat Microbiol*. 2020;5(7):929-942.
58. Rydberg EK, Salomonsson L, Hultén LM, et al. Hypoxia increases 25-hydroxycholesterol-induced interleukin-8 protein secretion in human macrophages. *Atherosclerosis*. 2003;170(2):245-252.
59. Sun MY, Taylor A, Zorumski CF, Mennerick S. 24S-hydroxycholesterol and 25-hydroxycholesterol differentially impact hippocampal neuronal survival following oxygen-glucose deprivation. *PloS One*. 2017;12(3):e0174416.
60. Marcello A, Civra A, Milan Bonotto R, et al. The cholesterol metabolite 27-hydroxycholesterol inhibits SARS-CoV-2 and is markedly decreased in COVID-19 patients. *Redox Biol*. 2020;36:101682.
61. Marathe SA, Sen M, Dasgupta I, Chakravortty D. Differential modulation of intracellular survival of cytosolic and vacuolar pathogens by curcumin. *Antimicrob Agents Chemother*. 2012;56(11):5555-5567.
62. Björkhem I, Diczfalusy U, Lövgren-Sandblom A, et al. On the formation of 7-ketocholesterol from 7-dehydrocholesterol in patients with CTX and SLO. *J Lipid Res*. 2014;55(6):1165-1172.
63. Guillemot-Legris O, Mutemberezi V, Buisseret B, et al. Colitis alters oxysterol metabolism and is affected by 4beta-hydroxycholesterol administration. *J Crohns Colitis*. 2019;13(2):218-229.

SUPPORTING INFORMATION

Additional supporting information can be found online in the Supporting Information section at the end of this article.

How to cite this article: Mergani A, Meurer M, Wiebe E, et al. Alteration of cholesterol content and oxygen level in intestinal organoids after infection with *Staphylococcus aureus*. *The FASEB Journal*. 2023;37:e23279. doi:10.1096/fj.202300799R